10.1 A 1.4-to-2.7GHz FDD SAW-Less Transmitter for 5G-NR Using a BW-Extended N-Path Filter-Modulator, an Isolated-BB Input and a Wideband TIA-Based PA Driver Achieving <-157.5dBc/Hz OB Noise

Gengzhen Qi[1], Haijun Shao[1], Pui-In Mak[1], Jun Yin[1], Rui P. Martins[1,2]

[1]University of Macau, Macau, China, [2]University of Lisboa, Lisbon, Portugal

For the sub-6GHz 5G New Radio (5G-NR), most FDD bands expand their signal bandwidth (BW) to 20MHz. In the NR-n74 Band (~1.45GHz), the duplex spacing (Δf) is only 48MHz. Such a small Δf/BW ratio (2.4) challenges the design of a multiband FDD SAW-less transmitter (TX) that must emit negligible noise at the nearby receiver (RX) band. Previous works [1,2] use high-order baseband (BB) filters, along with large bias currents, to suppress the out-of-band (OB) noise, but the power (>90mW) and area (~1mm^2) are large for an OB noise of -158dBc/Hz [2]. Although the charge-domain direct-launch digital TX [3] is more flexible and area-efficient (0.22mm^2), it entails off-chip baluns to extend the RF coverage, and has a limited output power (-3.5dBm). An alternative is to embed a gain-boosted N-path filter into the TX [4], such that high-Q bandpass filtering can be performed at a flexible RF. Still, the filtering effectiveness of [4] is moderate when the signal BW reaches 10MHz, showing an OB noise of just -154.5dBc/Hz.

This paper reports a multiband FDD SAW-less TX supporting a 20MHz BW. Its full schematic is detailed in Fig. 10.1.1. The key techniques are a BW-extended N-path filter-modulator (FIL-MOD), an isolated-BB input and a wideband TIA-based PA driver (PAD). Fully integrated in 28nm CMOS, our TX manifests a consistently low OB noise (<-157.5dBc/Hz) for different 5G-NR bands in 1.4 to 2.7GHz. Small chip area (0.31mm^2), sufficient output power (3dBm) and high TX efficiency (2.8 to 3.6%) are concurrently achieved.

BW-Extended N-Path FIL-MOD: In [4] the gain-boosted N-path filter is merged with the I/Q modulator to realize high-Q bandpass filtering at a flexible RF, relaxing the order of the BB filters. The proposed FIL-MOD brings the concept to a wider BW design. As shown in Fig. 10.1.2 (left), the I/Q modulation is realized by upmixing the 4-phase BB input (I/Q and differential) via SW_L. The 4-path SW_L is driven by a 4-phase 25%-duty-cycle LO (LO_{1-4}). The upmixed signal is then amplified by an RF gain stage ($-G_{m1}$). If $-G_{m1}$ is simply fed back by an N-path switched-capacitor (SC) negative-feedback network (NFN) made by $SW_{L,R}$ and C_F, the OB rejection will suffer from a hard tradeoff with the passband BW as in [4]. To decouple that we introduce an N-path SC positive-feedback network (PFN) made by SW_Z and C_Z. The parallelized PFN and NFN co-synthesize a complex-pole pair as explained by its analytical model in Fig. 10.1.2 (right). Owing to the bidirectional transparency of passive mixers, a BB lowpass response can be frequency-translated to RF as a bandpass one. By omitting $SW_{L,R}$ and SW_Z, the BB equivalence will be a $-G_{m1}$ surrounded by both PFN and NFN. The PFN is modeled as a negative-gain stage $-A_Z$ ($A_Z \approx 0.9$) in series with C_Z, whereas the NFN is only C_F. With the PFN, a 2nd-order input conductance is created $(Z_2)^{-1} \approx s^2 r_0 C_F C_Z + s(1-G_{m1} r_0 A_Z) C_Z$ when $\omega \ll (r_0 C_F)^{-1}$. Transferred from $V_{BB,I}(s)$ to $V_{BB,O}(s)$, the passband BW is expanded by the complex-pole pair. The natural frequency is given by $\omega_{BB}=[1/C_F C_Z r_0 Z_S(1+A_Z)]^{1/2}$, and the pole Q factor is proportional to C_Z/C_F. The overall transfer function $V_{RF}(s)/V_{BB,I}(s)$ exhibits a 4th-order bandpass response with the upper and lower natural frequencies given by $\omega_{C1,2}=\omega_{LO}\pm\omega_{BB}$. As a result, the passband BW is expanded along with an improved steepness of the OB rejection (Fig. 10.1.3, upper).

A simple NMOS device realizes the gain stage $-G_{m1}$, such that its bias and signal currents ($I_{O,P}$ and $I_{O,N}$) can be absorbed by its following TIA-based PAD. This co-design results in both linearity and TX efficiency. The differential implementation not only helps the output power, but also allows using cross-feedback capacitors C_1 to cancel the parasitic effects associated with $-G_{m1}$, trimming the passband shape. C_Z offers the design freedom to balance the OB rejection with the passband flatness at both $V_{I,P}$ and $V_{O,P}$ (Fig. 10.1.3, upper).

Isolated-BB Input: In the I/Q modulator of [4], the BB signals are injected to the gain-boosted N-path filter via a passive-RC network. Their mutual loading effects induce noise crosstalk and degrade the Q factor of the created bandpass response at RF. To hinder this effect, we propose in Fig. 10.1.1 an isolated-BB input (SW_B and C_B) that utilizes the adjacent phase of each non-overlap LO to time-interleave the operation of the BB injection and N-path filtering. This technique enhances the OB rejection of the BB noise (e.g., from the DACs) and preserves the BW of the FIL-MOD. The OB rejection (Fig. 10.1.3 lower) is improved at a small C_B (<2pF) when comparing it with the passive-RC-BB input. The lower limit of C_B is set by the passband BW. The on-resistance of SW_B (R_{SWB}) offers additional freedom to balance the BW of the FIL-MOD with the OB noise rejection (Fig. 10.1.3 lower).

Wideband TIA-Based PAD: A single-ended voltage-input amplifier as a PAD can suffer from low linearity and output power. Herein we propose a differential wideband TIA-based PAD to absorb the bias and signal currents of $-G_{m1}$. The differential RF outputs are combined by an on-chip 1.4:1 transformer (xfmr), shunted by a 5bit tunable C_T (0.1pF/step) to expand the RF coverage. Designed at a 1.8V supply and with the cross-coupling C_3, a small thick-oxide MOS transistor (M_3) is adequate to enhance the reverse isolation, reliability and voltage gain (by 4.6dB, from simulation). We use M_2 to isolate the two cross-coupling capacitors (C_1 and C_3) serving different purposes. The G_m linearizer ($-G_{m2,}$ biased in the triode region) improves the CIM_3 by cancelling the 3rd-order nonlinearity term of $-G_{m1}$ (biased in the saturation region). The entire $-Gm_1$ + PAD has a simulated OIP_3 of 26.7dBm. Variable-gain control, not realized in this work, can be applied to the PAD.

With the high-Q bandpass filtering at both $V_{I,P}$ and $V_{O,P}$, the LO-modulated phase noise can be effectively suppressed. From simulation, the LO generator only contributes 3.8% of the total OB noise (-158.5dBc/Hz) at 80MHz offset, whereas the major contributors are $-G_{m1}$ (27.8%), $SW_{L,R}$ (14.4%), SW_Z (7.2%) and PAD (18.2%). The remaining noise contributions are from the 50Ω load and bias circuit. SW_B only contributes 1.2%, and is hence downsized (6μm/30nm) to save the LO power. Due to the Miller effect created by the loop gain of $-G_{m1}$, small physical C_F (5pF) and $SW_{L,R}$ (20μm/30nm) are allowed to reduce the parasitic effects and LO power [5]. The simulated G_{m1} is 110.2mS and inverting gain from $V_{I,P}$ to $V_{O,P}$ is -1.6V/V.

The proposed fully integrated TX occupies 0.31mm^2 in 28nm CMOS (Fig. 10.1.7). By using a differential self-bias input-buffer amplifier, the LO generator shows a simulated power efficiency of ~4.8mW/GHz and a phase noise of -158.4dBc/Hz at 40MHz offset. We use transmission-gate switches to reduce the LO feedthrough and improve the linearity.

A high-Q bandpass response is consistently measured at different NR bands by simply tuning the LO frequency (Fig. 10.1.4). The flat passband BW is >20MHz. The output power is 3dBm at 2.535GHz (NR-n7 Band) with a 20MHz signal BW. The I/Q mismatch image and LO feedthrough are <-40dBc by manual calibration at the 4-phase BB sources (not the focus of this work). The $ACLR_1$ ($ACLR_2$) is -44.4dBc (-58.7dBc) and EVM is 1.9%. The output noise is -158dBc/Hz at 120MHz offset, and CIM_3 (CIM_5) is -54dBc (-64.2dBc). The results are consistent at 1.88GHz (NR-n2) and 1.4485GHz (NR-n74) as summarized in Fig. 10.1.5. The OB noise degradation is ≤1.5dB under power backoff. The $ACLR_{1,2}$ vary <2dB regardless of the signal BW of 10MHz or 20MHz. The power consumption increases from 55.1mW at the NR-n74 Band, to 70.5mW at the NR-n7 Band. The TX can support a wider signal BW >20MHz, but it has to trade-off with OB rejection (Fig. 10.1.3, lower left). To improve both the OB noise and signal BW, we can incorporate a better BB DAC and more BB filtering.

Figure 10.1.6 summarizes the chip performance and compares it with the prior art [3,4,6]. This work demonstrates a number of performance advantages. Although [3] reports a smaller die area than this work, it requires off-chip baluns to combine the differential outputs, and its output power is 6.5dB lower. Comparing with [4], this work supports a 2× wider signal BW and achieves a 3dB lower OB noise and a 4dB higher output power. With similar output power and OB noise as [6], this work shows higher area efficiency (3.3×) and TX efficiency (56%).

Acknowledgements:
The work is funded by MYRG2017-00223-AMSV and Macau FDCT - SKL Fund.

References:
[1] V. Giannini et al., "A Multiband LTE SAW-Less Modulator with -160dBc/Hz RX-Band Noise in 40nm LP CMOS," *ISSCC*, pp. 374-376, Feb. 2011.
[2] N. Codega et al., "A Current-Mode, Low Out-of-Band Noise LTE Transmitter with a Class-A/B Power Mixer," *IEEE JSSC*, vol. 49, no. 7, pp. 1627-1638, July 2014.
[3] P. Filho et al., "A 0.22mm^2 CMOS Resistive Charge-Based Direct-Launch Digital Transmitter with -159dBc/Hz Out-of-Band Noise," *ISSCC*, pp. 250-252, Feb. 2016.
[4] G. Qi et al., "A 0.038mm^2 SAW-Less Multiband Transceiver Using an N-Path SC Gain Loop," *IEEE JSSC*, vol. 52, pp. 2055-2070, Aug. 2017.
[5] G. Qi et al., "A SAW-Less Tunable RF Front-End for FDD and IBFD Combining an Electrical-Balance Duplexer and a Switched-LC N-Path LNA," *IEEE JSSC*, vol. 53, no. 5, pp. 1431-1442, May. 2018.
[6] Q. Liu et al., "A 1.4-to-2.7GHz High-Efficiency RF Transmitter with an Automatic 3FLO-Suppression Tracking-Notch-Filter Mixer Supporting HPUE in 14nm FinFET CMOS," *ISSCC*, pp. 172-174, Feb. 2018.

 978-1-7281-3205-1/20/$31.00 ©2020 IEEE

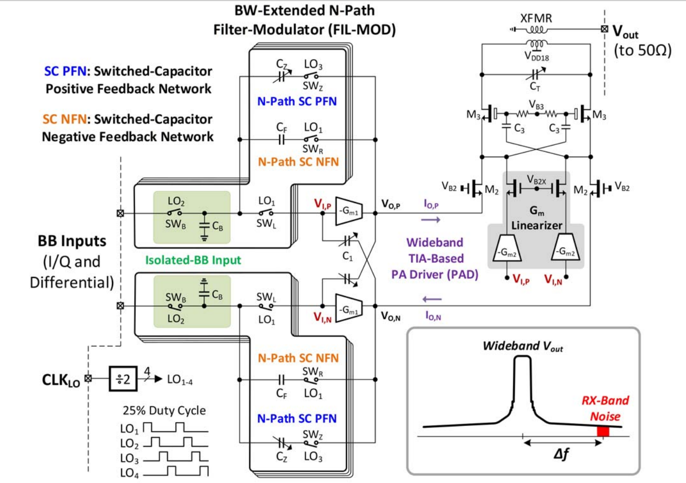

Figure 10.1.1: Proposed fully integrated multiband SAW-less TX for 5G NR. It features a BW-extended N-path FIL-MOD, an isolated-BB input, and a wideband TIA-based PAD to absorb the bias and signal currents of $-G_{m1}$ for better linearity and TX efficiency.

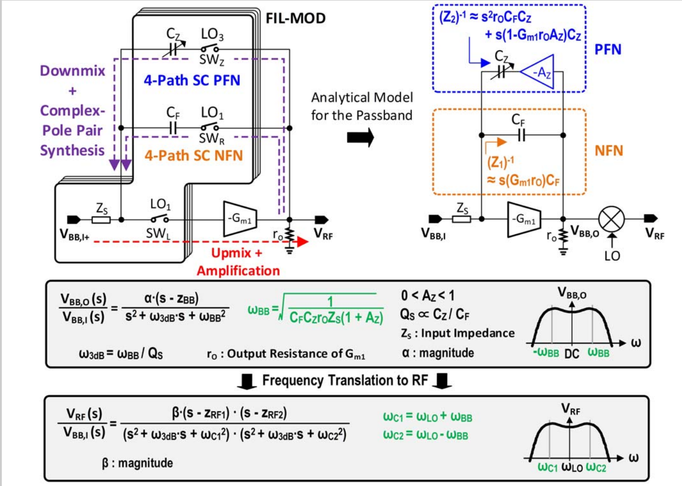

Figure 10.1.2: The FIL-MOD is realized by merging a gain-boosted N-path filter into the I/Q modulator to realize tunable high-Q bandpass filtering at flexible RF. The passband BW is widened by using the 4-path SC NFN + PFN to form a complex-pair pole with $-G_{m1}$.

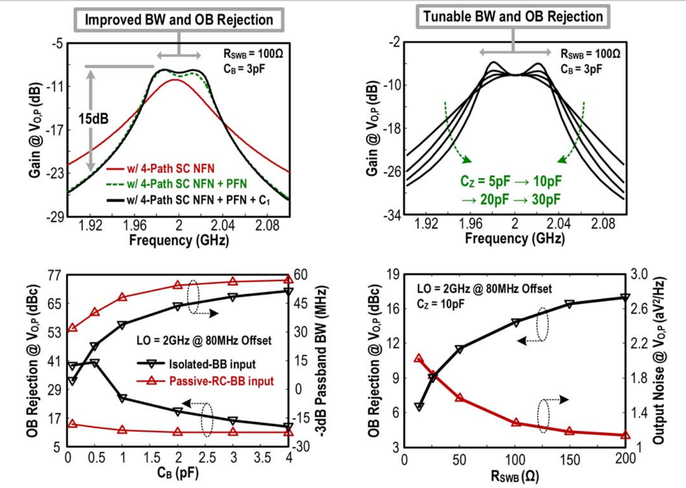

Figure 10.1.3: *Upper:* Simulated BW-extended passband at RF, and the tunable BW and OB rejection for different C_Z. *Lower:* Isolated-BB input improves OB rejection compared to passive-RC BB input, and R_{SWB} allows balancing the OB rejection and OB noise at $V_{O,P}$.

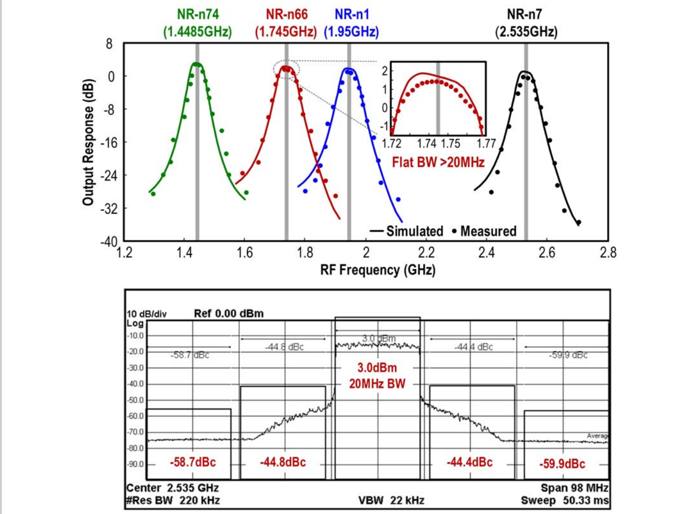

Figure 10.1.4: *Upper*: Measured and simulated LO-defined bandpass responses at different NR bands. *Lower*: Measured output spectrum for NR-n7 (2.535GHz) with a 20MHz BW.

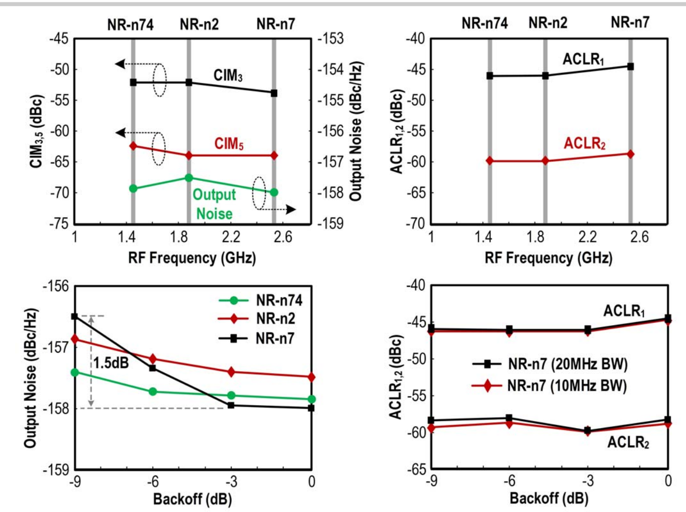

Figure 10.1.5: *Upper*: Measured $CIM_{3,5}$, output noise and $ACLR_{1,2}$ for different NR bands. *Lower*: Output noise and $ACLR_{1,2}$ for 10 and 20MHz signal BWs under power backoff.

	This Work			ISSCC'18 [6]	JSSC'17 [4]	ISSCC'16 [3]
TX Techniques	**Isolated-BB input + BW-Extended N-Path Filter-Modulator + Wideband TIA-based PAD**			Tracking-Notch-Filter Mixer + PAD	N-Path SC Gain Loop + Wideband PAD	Resistive QDAC + Passive Mixer
Full Integration	**Yes**			Yes	Yes	No
RF Range (GHz)	**1.4 to 2.7**			1.4 to 2.7	0.7 to 2	0.9, 2.4
Frequency Bands	**NR-n74 (1.4485GHz)**	**NR-n2 (1.88GHz)**	**NR-n7 (2.535GHz)**	HPUE-B41 (2.535GHz)	LTE-B2 (1.88GHz)	2.4GHz
RF BW (MHz)	20	20	20	20	10	20
Output Power (dBm)	**3.0**	**3.1**	**3.0**	3.1	-1#	-3.5
Power Cons. (mW)	55.1	60.2	70.5	113.2	38.4	24.8
TX Efficiency (%)	**3.6**	**3.4**	**2.8**	1.8	2.1	1.8
Output Noise (dBc/Hz) @ Δf (MHz)	**-157.8 @ 48**	**-157.5 @ 80**	**-158 @ 120**	-157.8 @ 80	-154.5 # @ 80	-158.9 @ 45
CIM_3 (dBc)	-52.3	-52.5	-54	-59.6	-52	<-50
$ACLR_1$ (dBc)	-45.4	-45.6	-44.4	-44.7	-40.3	-47
EVM (%)	1.9	1.8	1.9	No data	2.0	<1.6
Active Area (mm^2)	**0.31**			1.04	0.038 #	0.22 &
Supply Voltage (V)	1, 1.8			No data	1.1, 2.5	0.9, 1.1
CMOS Tech. (nm)	28			14	65	28

& Need off-chip baluns for multiband coverage, # Inductorless single-ended TX shows inadequate output power & high OB noise

Figure 10.1.6: Performance summary and benchmark with the state-of-the-art.

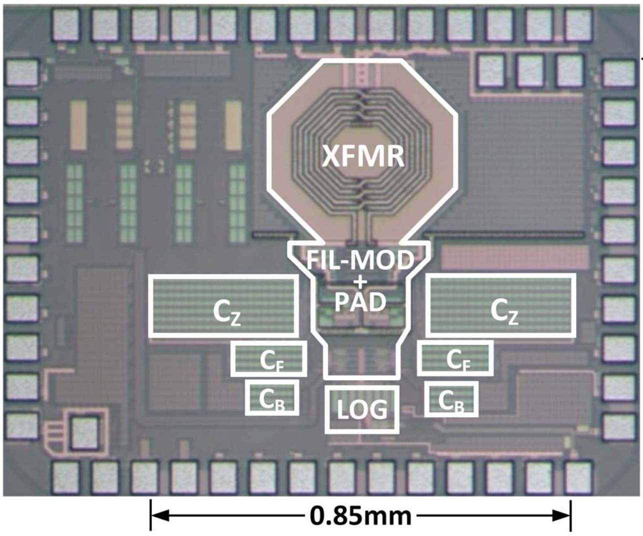

Figure 10.1.7: Die micrograph of the fabricated TX in 28nm CMOS.

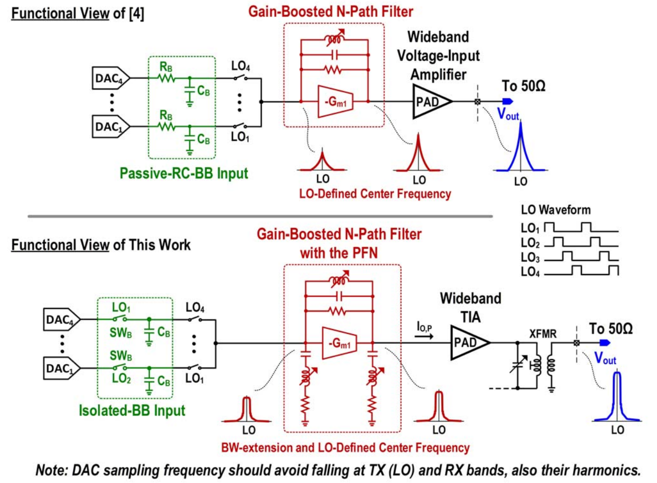

Figure 10.1.S1: *Upper:* [4] is based on the passive-RC-BB input, gain-boosted N-path filter and voltage-input amplifier as the PAD. *Lower:* This work features the isolated-BB input, gain-boosted N-path filter with BW extension, and a wideband TIA as the PAD.

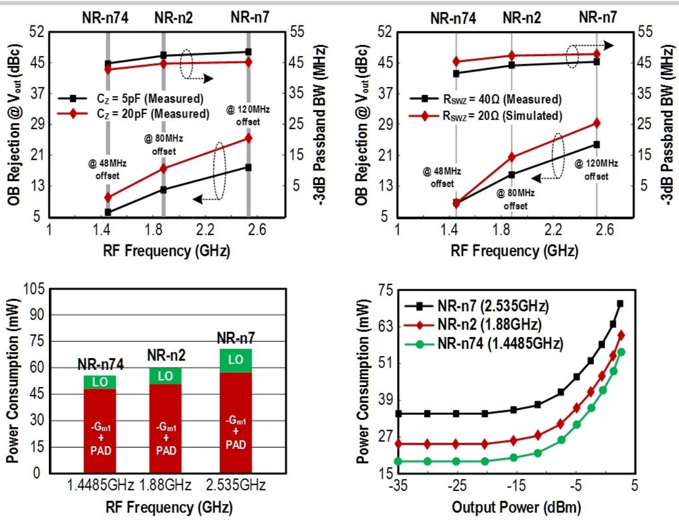

Figure 10.1.S2: *Upper*: Measured OB rejection and -3dB passband BW under different C_Z and SW_Z. *Lower*: Power consumption at different NR bands and under power backoff.

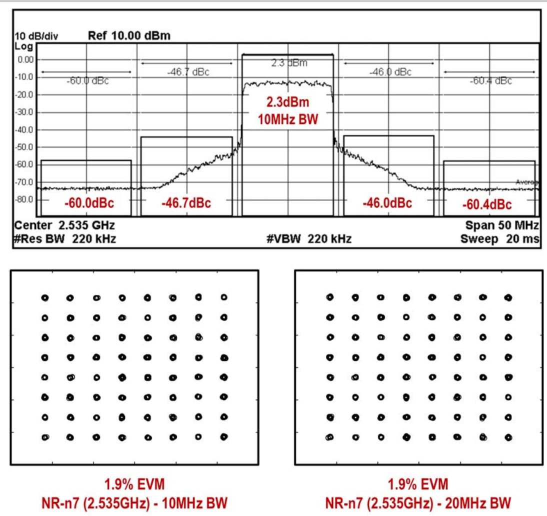

Figure 10.1.S3: Measured output spectrum and constellation diagram in the NR-n7 Band. The constellation diagram with a 20MHz BW supplements the output spectrum in Fig. 10.1.4.